

Estimating the Diapycnal Transport Contribution to Warm Water Volume Variations in the Tropical Pacific Ocean

JACLYN N. BROWN

Wealth from Oceans National Research Flagship, Hobart, Tasmania, Australia

ALEXEY V. FEDOROV

Department of Geology and Geophysics, Yale University, New Haven, Connecticut

(Manuscript received 27 November 2007, in final form 19 July 2009)

ABSTRACT

Variations in the warm water volume (WWV) of the equatorial Pacific Ocean are considered a key element of the dynamics of the El Niño–Southern Oscillation (ENSO) phenomenon. WWV, a proxy for the upper-ocean heat content, is usually defined as the volume of water with temperatures greater than 20°C. It has been suggested that the observed variations in WWV are controlled by interplay among meridional, zonal, and vertical transports (with vertical transports typically calculated as the residual of temporal changes in WWV and the horizontal transport divergence). Here, the output from a high-resolution ocean model is used to calculate the zonal and meridional transports and conduct a comprehensive analysis of the mass balance above the 25 kg m⁻³ σ_θ surface (approximating the 20°C isotherm). In contrast to some earlier studies, the authors found that on ENSO time scales variations in the diapycnal transport across the 25 kg m⁻³ isopycnal are small in the eastern Pacific and negligible in the western and central Pacific. In previous observational studies, the horizontal transports were estimated using Ekman and geostrophic dynamics; errors in these approximations were unavoidably folded into the estimates of the diapycnal transport. Here, the accuracy of such estimates is assessed by recalculating mass budgets using the model output at a spatial resolution similar to that of the observations. The authors show that errors in lateral transports can be of the same order of magnitude as the diapycnal transport itself. Further, the rate of change of WWV correlates well with wind stress curl (a driver of meridional transport). This relationship is explored using an extended version of the Sverdrup balance, and it is shown that the two are correlated because they both have the ENSO signal and not because changes in WWV are solely attributable to the wind stress curl.

1. Background

One of the leading paradigms for the El Niño Southern–Oscillation phenomenon is the recharge–discharge oscillator (Jin 1997; Meinen and McPhaden 2000; Jin and An 1999). This description of ENSO is based on the zonal redistribution of water along the equator associated with El Niño and La Niña, and a recharge and discharge of warm water in the equatorial Pacific preceding each event. The recharge and discharge can be measured as variations in the volume of water warmer than 20°C, also known as warm water volume (WWV).

The recharge of the WWV occurs approximately six months to one year in advance of an El Niño event, and potentially could be used as a predictive tool.

Prior to an El Niño event, the equatorial Pacific recharges with warm water, increasing the mean depth of the thermocline along the equator and preconditioning the ocean for an El Niño event to occur. Initially, the buildup of warm water tends to take place over the central-western part of the Pacific (Meinen and McPhaden 2000, 2001, hereafter MM01). During the El Niño event the warm water is advected to the eastern part of the basin, deepening the thermocline in the east, and therefore resulting in a flatter thermocline across the basin. Throughout the El Niño event, the flattened thermocline generates an anomalous poleward geostrophic transport, reducing the mean depth of the thermocline (Jin and An 1999; Bosc and Delcroix 2008). By the end of the El Niño, the

Corresponding author address: Jaclyn N. Brown, GPO Box 1538, Centre for Australian Weather and Climate Research, Hobart, Tasmania 7001, Australia.
E-mail: jaci.brown@csiro.au

ocean is left in a “discharged” state, with a raised thermocline across the basin, primed for a La Niña event to occur.

Previous descriptions of the oscillator (see Fig. 1 of Meinen and McPhaden 2000) attributed the recharge and discharge of the equatorial ocean to meridional Sverdrup transport, but later work by MM01 and Alory and Delcroix (2002) showed the importance of zonal transports as well.

The transports in and out of the equatorial Pacific to generate these WWV changes have been studied in terms of Kelvin and Rossby waves and geostrophic and Ekman dynamics (Alory and Delcroix 2002; MM01). MM01 used the data from Tropical Atmosphere Ocean moorings to explore the relative contributions of the zonal, meridional, and diathermal transports. They found that the recharge prior to the 1997–98 El Niño accumulated from an anomalous decrease in southward transport across 8°S into the western and central Pacific, along with an increase in eastward transport across 156°E. After the El Niño event, according to MM01, approximately half of the warm water was lost via meridional transports while the rest was lost to downward diathermal mass flux.

MM01’s study relied on using available ocean observations to estimate geostrophic and Ekman flows. The residual from the sum of these geostrophic and Ekman transports was then attributed to a diathermal transport. Consequently, errors in the horizontal transports were unavoidably folded into the estimates of vertical fluxes.

Alory and Delcroix (2002) used satellite altimetry and linear models to estimate the horizontal transports. They developed a comprehensive dynamical description of the Kelvin and Rossby waves in the oscillator paradigm, attributing meridional and zonal transports to equatorial waves that were generated by wind anomalies. They argued that WWV changes were due to both zonal and meridional transports, but could not quantify the role of the diapycnal transports.

Clarke et al. (2007), also using observations and the results of MM01, show that the rate of change of the WWV is correlated with the wind stress curl (which gives an estimate of meridional transport). From this correlation they conclude that the recharge and discharge can be explained primarily by the meridional transports. They argue that zonal flows therefore do not affect the volume of water above the 20°C isotherm and must be balanced by diathermal fluxes. These conclusions, however, are based on a limited amount of data and several approximations made to estimate the transport as in MM01. Furthermore, the work by Kessler et al. (2003) and Brown et al. (2007a, 2010), showing the importance of nonlinear advection in the equatorial Pacific, highlights the need to reevaluate these findings.

In each of these observational studies diathermal or diapycnal transports are not measured directly, but calculated as residuals of the estimates for horizontal flows. In the present study we use output from a high-resolution ocean GCM to calculate diapycnal flows and determine the extent to which they contribute to WWV variations on ENSO time scales. We focus on the period October 1992–December 1998, following the observational study of MM01. First, we confirm that the recharge and discharge occur largely due to a combination of zonal and meridional transports. The diapycnal contribution to the mass balance is shown to be almost negligible in the western-central Pacific and relatively small in the east, at least across the $25 \text{ kg m}^{-3} \sigma_\theta$ surface, which approximates the thermocline in the model.

Previous results have hinged upon the reliability of observations and estimates of transports, while our results are contingent on the fidelity of the model. To assess the reliability of the approximations used by the observational studies, we redo their calculations using a similar subset of the model output and assess how well we can recover the actual model transports. We find that the largest errors occur in zonal transport estimates within a few degrees of the equator. Diapycnal transports cannot be reliably estimated based on the present observational network because at 5–10 Sv ($\text{Sv} \equiv 10^6 \text{ m}^3 \text{ s}^{-1}$), they are of similar magnitude to the errors caused by the dynamical approximations used to deduce the meridional and zonal transports.

2. Ocean model data and processing

The model is a global version of the Australian Community Ocean Model, version 3 (ACOM3) [see Schiller (2004); Schiller and Godfrey (2003) for further details] and is based on the Geophysical Fluid Dynamics Laboratory (GFDL) Modular Ocean Model 3 (MOM3) code (Pacanowski and Griffies 2000). The model output covers only a 6-yr period (1992–98); however, it has the advantage of being forced with the high-resolution European Remote Sensing Satellite (ERS) scatterometer winds as provided by IFREMER (<http://www.ifremer.fr/cersat>; see Bentamy et al. 1999). These winds have sufficient resolution to capture the wind stress curl features near the equator, which will be important to our analysis. Other wind stress products have been shown to miss a patch of positive curl near the equator (Kessler et al. 2003).

Model resolution is $\frac{1}{3}^\circ$ in latitude and $\frac{1}{2}^\circ$ in longitude. There are 36 vertical levels, of which the top 10 are 10 m thick and increase downward with a thickness of 225 m by the 1000-m depth. Model output is taken as 3-day averages.

A nonlinear Smagorinsky biharmonic mixing scheme (Griffies and Hallberg 2000) was used for horizontal

momentum and tracer mixing. In the vertical, a hybrid Chen mixing scheme (Schiller et al. 1998; Power et al. 1995) is applied with a Niiler–Kraus-like bulk mixed layer (Niiler and Kraus 1977) near the surface, and gradient Richardson number mixing below.

Surface fluxes, apart from incoming shortwave radiation, are calculated by coupling the OGCM to an atmospheric boundary layer model of Kleeman and Power (1995) described in Schiller and Godfrey (2003). The boundary layer model consists of a single-layer atmosphere (boundary layer as well as a portion of the cloud layer) that is in contact with the surface.

Net solar shortwave radiation and precipitation are input to an atmospheric boundary layer model (ABLM) among other parameterizations. The ABLM prognostically calculates air temperature in the boundary layer above the surface. Surface latent and sensible heat fluxes are then diagnosed using the bulk formulae. Freshwater fluxes were calculated from the simulated evaporation (latent heat) together with precipitation from the Carbon Dioxide Information Analysis Center (CDIAC) Microwave Sounding Unit (MSU) precipitation dataset. More details can be found in Schiller (2004).

The model that we are using is compared with observations from Johnson et al. (2002, see Fig. 1) and is discussed in more detail in Brown (2005) and Brown et al. (2007a,b). The Equatorial Undercurrent (EUC) is approximately 10% weaker in the model in the east, up to 50% weaker in the west, and has its maximum lying 20 m deeper (Fig. 1). The model does not fully capture the strength of the surface south equatorial currents, being 0.1 m s^{-1} weaker than the observations in most places. The North Equatorial Countercurrent lies between 4° and 8°N , and its magnitude of $0.2\text{--}0.4 \text{ m s}^{-1}$ is consistent with observations. Its position is significant to whether it is included in our analysis. The North Equatorial Countercurrent in the model shifts equatorward midyear, joining with the EUC, which is not reflected in the observations of Johnson et al. (2002). Kessler and Taft (1987), however, did find similar a connection between the two currents.

Throughout the paper the model results are compared to observational data [prepared by N. Smith's group at the Australian Bureau of Meteorological Research (BMRC)], as used by MM01. The development and preparation of the dataset are discussed in Smith et al. (1991), Smith (1991, 1995a,b), and Meyers et al. (1991).

3. Results

a. Defining the WWV

WWV is generally defined as the volume of water warmer than 20°C within 5° of latitude either side of the

equator. The 20°C isotherm was chosen to approximate the thermocline, and thus this description relates to ocean dynamics in the $1\frac{1}{2}$ -layer shallow-water model. We will refer to this measure as an “isothermal” WWV. Long records of salinity in the tropics are not available and so an “isopycnal” WWV cannot be calculated. However, since ocean general circulation models contain comprehensive temperature and salinity information, it is natural to calculate a volume above a certain isopycnal (or isopycnal WWV). A mass balance can then be calculated by considering horizontal transports above the moving isopycnal surface. Any imbalance between the rate of change of the isopycnal WWV and the horizontal transports is therefore primarily due to diapycnal transports.

It is possible that variations in surface precipitation (P) and evaporation (E) might contribute to the volume balance. MM01 showed, however, that the mean $E - P$ over our region of interest gives a surface volume transport of around 0.05 Sv . They argue that, even if this value is an order of magnitude too small, the input through the ocean surface is still negligible compared to the total volume balance.

To ensure that our *isopycnal* WWV study is comparable to the results of *isothermal* WWV calculations, we need to choose an isopycnal that closely matches the thermocline in the model, thereby giving us the physical lower boundary for WWV calculations. The 20°C isotherm is not necessarily a good proxy for the thermocline depth in a model study, as the model's ocean thermal structure can be somewhat different from what is observed. In fact, the 21°C isotherm in our model seems to be a better representation of the model's thermocline and the pycnocline (Fig. 1). Likewise, the $25 \text{ kg m}^{-3} \sigma_\theta$ surface appears to be a good proxy for the pycnocline in the model as well as the optimum choice for the lower boundary in WWV calculations (for reasons explained below).

One of the differences between our model and the observations is the mean depth of the Equatorial Undercurrent, shown in Fig. 1 for the eastern and western Pacific at 110° and 170°W . Although the model places the EUC about 20 m deeper than observed, the density profile in the model relative to the EUC is consistent with the observations. For example, the 25.0 kg m^{-3} isopycnal lies just above the core of the EUC in both observations and model, regardless of depth.

In the observations, the 20°C isotherm (Fig. 1a,c) aligns with the 25.0 kg m^{-3} isopycnal, sitting within the top part of the EUC. This isopycnal and isotherm pair also appears to lie near to the level of the maximum vertical density gradient (not shown explicitly), a measure of the pycnocline depth. This suggests that in the

Zonal Currents, Potential Density and Potential Temperature

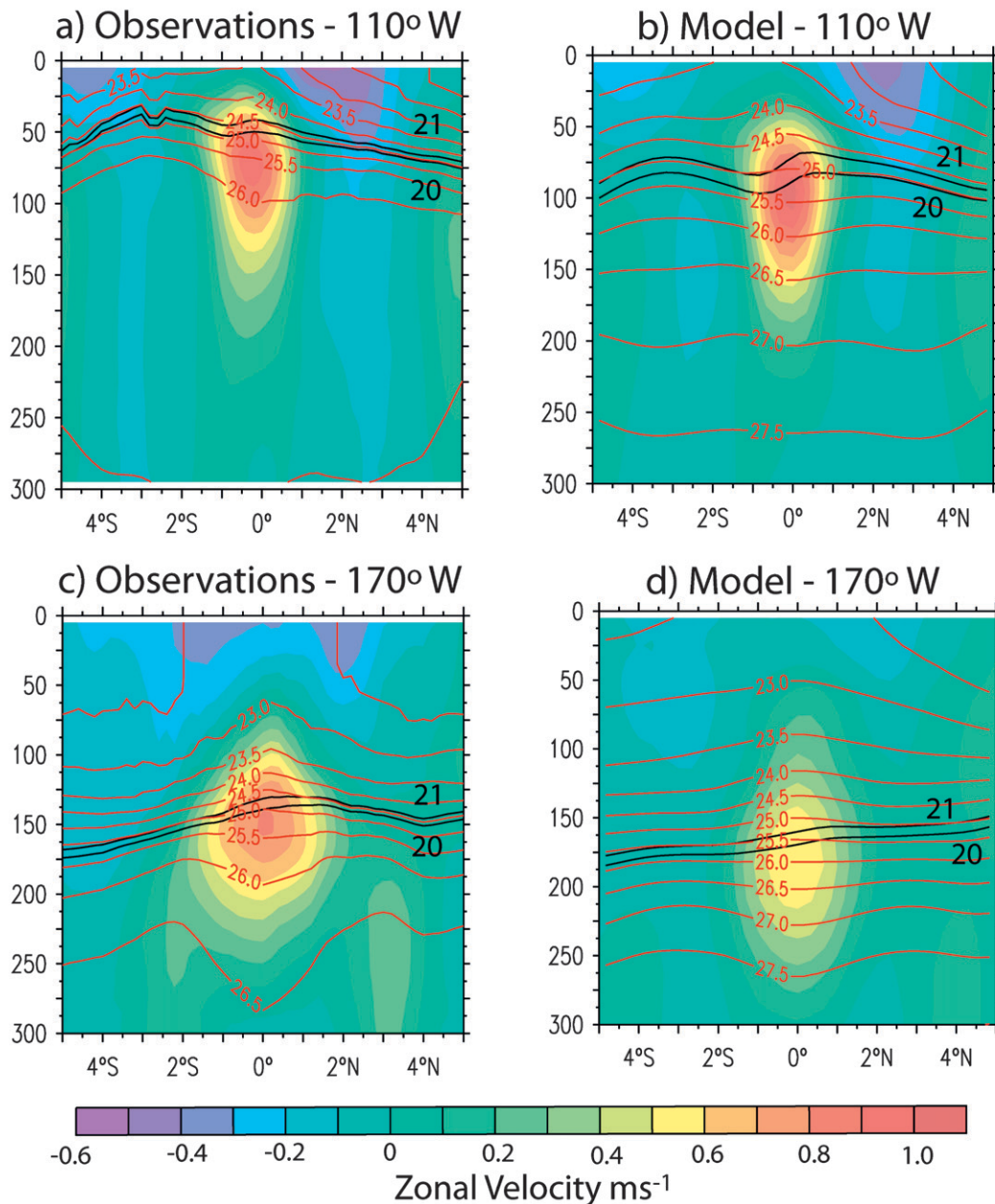


FIG. 1. The Equatorial Undercurrent and ocean vertical stratification in observations and the model: (a),(c) The observed mean structure of the EUC (color) with isolines of potential density (red) for the eastern equatorial Pacific (at 110°W) and for the western equatorial Pacific (at 170°W) and (b),(d) the model EUC and potential density isolines at 110° and 170°W. Also shown are the 20° and 21°C isotherms (black). Observational data represents an average from 1985 to 2000 (Johnson et al. 2002).

observations the isopycnal WWV calculated from the surface to 25 kg m^{-3} would be equivalent to an isothermal WWV measured to 20°C.

What is the corresponding measure of WWV in the model? Clearly the 20°C isotherm is not the correct

measure of WWV in the model, as it sits within the maximum of the EUC (Figs. 1b,d), below the pycnocline. The model's 25.0 kg m^{-3} isopycnal lies above the EUC core as did the 25.0 kg m^{-3} isopycnal in the observations. This temperature–isopycnal mismatch could

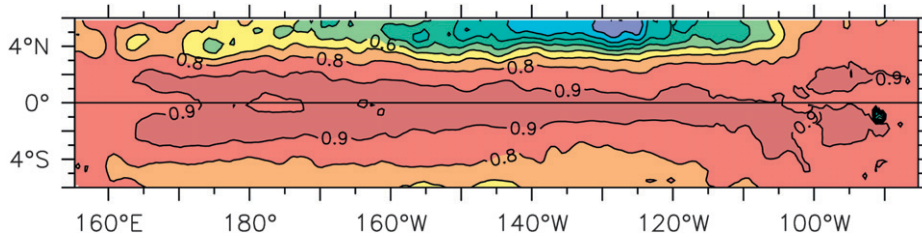


FIG. 2. The temporal correlation between the depth of the model 21°C isotherm and that of the 25.0 kg m⁻³ density surface as a function of longitude and latitude. At the depths studied, the temporal variability of the isotherms in the equatorial strip correlates highly with the variability of the isopycnals, making them reasonably interchangeable. This relationship breaks down north of 4°N where the ITCZ introduces strong salinity variations. The interval between adjacent contour lines is 0.1.

be due to either the model being too warm in this region, having an error in the salinity data, or both.

The model's 24.5 kg m⁻³ surface is a similar depth to the observed 20°C isotherm, but it cannot be used as the WWV cutoff because it is too shallow and does not incorporate the full dynamics down to the thermocline and EUC, as in the observations. (Note that choosing deeper isopycnals, such as 25.5 kg m⁻³, is also not an option, as they lie below the core of the model's EUC core and therefore incorporate different dynamics, and salinity variations become important.)

Choosing the correct isopycnal is a balance between two competing factors—too deep an isopycnal will not capture the isothermal movements of the pycnocline, and too shallow a thermocline will be influenced by processes such as surface fluxes and the nighttime ocean mixed layer. Furthermore, isopycnals that outcrop into the mixed layer and surface within our region of interest (such as 24.5 kg m⁻³) would also be affected by cross-isopycnal transports induced by horizontal mixing.

In summary, in our model we could take either the 21°C isotherm or 25 kg m⁻³ isopycnal as the lower boundary for WWV calculations, which is supported by the high temporal correlation between the two surfaces (Fig. 2). However, since one of our goals is to diagnose diapycnal transports, we will choose the 25 kg m⁻³ isopycnal as the demarcation. (Later, we will show that the interannual WWV index based on the observed 20°C isotherm correlates strongly with the model index based on this isopycnal.)

b. Transport balance

First, we evaluate the mass balance for two large boxes in the equatorial Pacific—important for the ocean recharge and discharge (Fig. 3). Both boxes cover the area between 5°S and 5°N [in line with the Alory and Delcroix (2002) study]. Longitudinally, the west box extends from 156°E to 140°W and the east box from 140°W to the South American coastline. The borders of

the west box were chosen to be comparable with MM01 and to avoid the strong western boundary currents and coastline of the Maritime Continent. Setting the western boundary at 156°E allows us to consider the net effect of these boundary currents as a zonal flow contribution to WWV.

The WWV for each box is evaluated by calculating the water volume down to the instantaneous depth of the 25.0 kg m⁻³ isopycnal and then integrating horizontally over the box area. Similarly, the horizontal transports across the borders of each box are integrated down to the same isopycnal, as described in Brown et al. (2007a). The balance of water in the west box is

$$\begin{aligned} \frac{\partial \text{WWV}}{\partial t} = & - \iint v(y = 5^\circ\text{N}) dx dz + \iint v(y = 5^\circ\text{S}) dx dz \\ & + \iint u(x = 156^\circ\text{E}) dy dz \\ & - \iint u(x = 140^\circ\text{W}) dy dz + \text{diapycnal flow}, \end{aligned} \quad (1)$$

where u , v are the zonal and meridional velocities. The diapycnal flow is the imbalance between the horizontal divergence and the change in WWV. The balance for the east box is similar but has no zonal flow through the eastern ocean boundary against the coast of South America.

For the mean state of the system, for which the rate of change of WWV is zero, net zonal transports are eastward into each box (Fig. 3). The meridional flow is northward in the west box and southward in the east box [further discussion of the mean state of this model can be found in Brown et al. (2007b)]. The small residual between the horizontal transports implies a contribution from either diapycnal transports or precipitation and evaporation. Assuming $E - P$ is small (see the previous discussion), 2.2 Sv of diapycnal upwelling is required to close the balance in the west box. The east box requires three times as much (6.6 Sv), which reflects the shoaling of the thermocline in

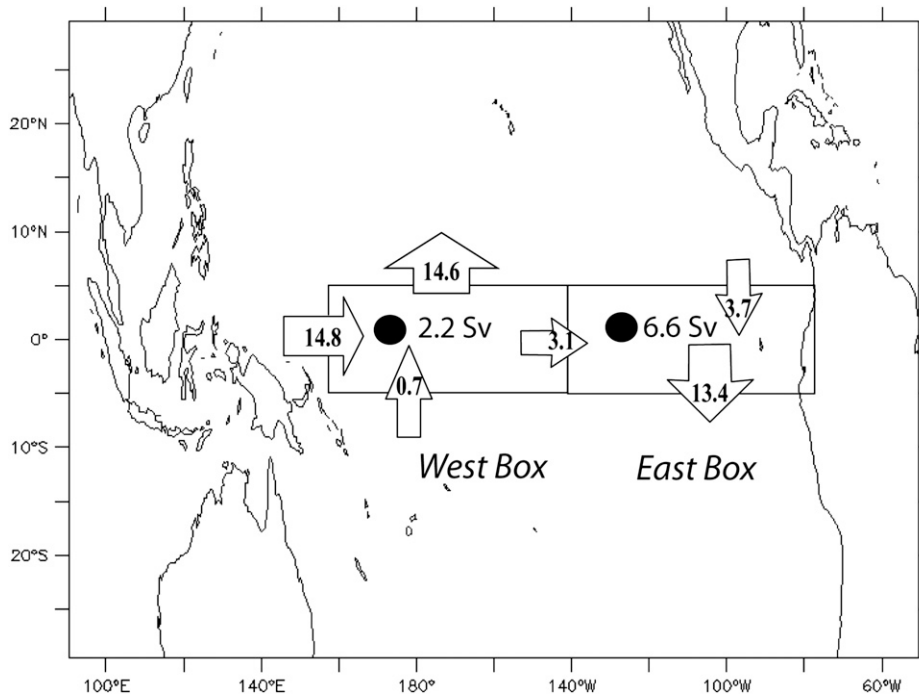


FIG. 3. The two boxes in the tropical Pacific Ocean used for calculating mass balances. The west box extends from 156°E to 140°W and the east box from 140°W to the coast of South America. Mean values of horizontal transports (Sv) at the box boundaries are for flow above the $25.0 \text{ kg m}^{-3} \sigma_\theta$ surface. The corresponding upward diapycnal transports across this isopycnal are 2.2 Sv and 6.6 Sv (indicated by black dots).

this region, the strong Ekman upwelling, and potentially the relatively strong air–sea heat fluxes.

Note that the values of mean diapycnal upwelling in the east box depend on the isopycnal chosen for the calculations. More diapycnal upwelling occurs across isopycnals that are shallower than 25 kg m^{-3} . However, those isopycnals do not describe the model ocean pycnocline, and we are interested in calculating diapycnal transports across the pycnocline. The mean diapycnal upwelling in this particular model across a range of isopycnals is discussed in Brown et al. (2007a,b).

Also note that our estimates of the diapycnal transport incorporate both mass transport across the pycnocline and the effect of ocean heat fluxes. The west box is deep enough for these heat fluxes to not alter the pycnocline depth significantly; however, the east box has a thermocline sufficiently shallow to be influenced by shortwave radiation. About one-third of the diapycnal effects on the mean state of the tropical ocean may be due to shortwave radiation directly heating the basin (Iudicone et al. 2008). We anticipate that the vertical diapycnal transports we calculate would have roughly the same contribution from the heat fluxes.

The interannual variability of the *isothermal* WWV was studied in the past because it is a useful predictor of

ENSO events. Our *isopycnal* WWV index is equally good: it correlates with the isothermal WWV with a coefficient of 0.92 in the west and 0.87 in east (Fig. 4). In the west box, the WWV indices lead the Niño-3.4 index by roughly seven months, as shown by MM01. In the east box, the WWV anomalies occur around the same time as Niño-3.4.

WWV indices are effective ENSO predictors because they quantify the “recharge” of the equatorial Pacific before an El Niño event. Where does the water come from to recharge the boxes? In the west box the rate of change of isopycnal WWV (dashed pink line in Fig. 5) can be accounted for by the horizontal divergence (blue line). There is very little need for diapycnal transports (green line) to close the balance and we can claim that the flow is largely adiabatic. In the east box the discrepancy between the change in volume and the net horizontal transport in and out of the box is larger, though it does not appear to exceed 10 Sv. The standard deviation of the diapycnal transport in the east box is 4.2 Sv, which is much smaller than the variance of the net horizontal transport with a standard deviation of 15.4 Sv.

Clearly the horizontal divergence dominates the ENSO recharge in our model. Next, we will briefly explore the role of the zonal and meridional transports separately, taking the strong 1997–98 El Niño as a case study. In

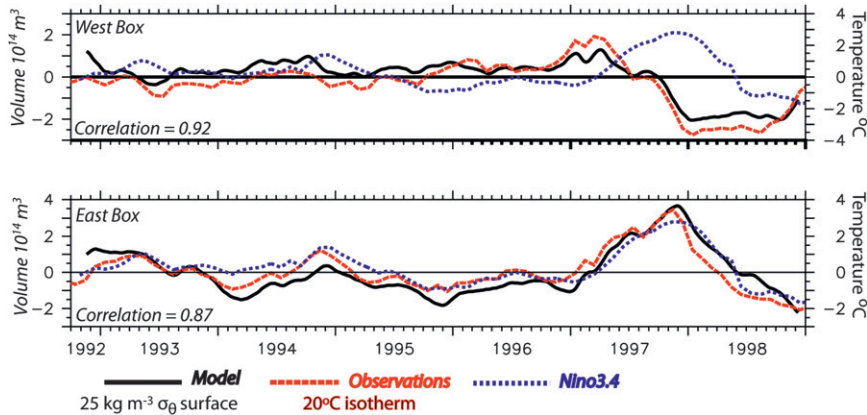


FIG. 4. Comparison of WWV indices for the (top) west box and (bottom) east box. The isothermal WWV (10^{14} m^3) for observations (red-dashed line) is measured from the surface to the 20°C isotherm. The isopycnal WWV in our model (black line) is measured to the $25 \text{ kg m}^{-3} \sigma_\theta$ surface. Overlaid is the Niño-3.4 index (blue-dotted line). Observations are monthly (courtesy of N. Smith, BMRC); the model temporal resolution is 3 days, with a 15-point smoothing. Correlation coefficients between the isothermal and isopycnal WWV indices are shown in the lower-left corner of each panel.

Fig. 6 the total zonal, meridional, and diapycnal transports are plotted for each box and for the two boxes combined (solid lines) and compared to their mean values (dashed lines). Note that each side of the box is not considered separately; instead, we calculate the net transport (zonal and meridional) for each case.

In the east box (Fig. 6b), the rate of change of WWV (black line) throughout 1996 is near zero. In 1997, the zonal transport from the west box to the east box accelerates, increasing the WWV; the zonal transport is maintained throughout 1997 and then reverses in 1998. There is a short pause in the eastward transport in July 1997 when the west box appears to be recharging again, deepening the thermocline, but this lasted only for a few months.

The meridional transport anomaly (red line) removes water from the east box in mid-1997 into 1998. The net effect by the end of 1997 is decreased WWV as a result of warm water drainage by the combined meridional and zonal transports. As discussed earlier, the diapycnal transport variations (green line) are very small in comparison.

In the west box, the horizontal transports exhibit a more complex behavior (Fig. 6a). In mid-1996 the west box is in a recharged state that was generated earlier. The zonal (blue) and meridional (red) net transports are near their average strength—the net zonal transport adding water to the box and the net meridional transport removing it. Toward the end of 1996 the meridional transport out of the box weakens, allowing the WWV in the west box to increase (indicating an even stronger recharge). The start of El Niño in February 1997 is signaled as the west box begins its discharge into the eastern

Pacific. The warm water discharge throughout 1997 results from the changes in both meridional and zonal transports.

As has been shown, the zonal transports are as important as the meridional ones in this process and should not be neglected, particularly when looking at the west and east boxes separately. Even if we considering the boxes combined (Fig. 6c), both meridional and zonal transports are essential for WWV variations. In fact, the rate of change of WWV correlates with the meridional transport convergence with a correlation coefficient of only 0.47.

c. Estimating horizontal transports from available observations

We will now use model output, on the same spatial grid as the available ocean data, to determine the sampling errors that would occur when estimating diapycnal transport from the observations. Studies with observational data depend on a number of assumptions and approximations to calculate ocean currents. At the end, the diapycnal transport is estimated as a small difference between these large, estimated horizontal transports; small errors in calculating them therefore become critical.

We have taken the output from the model in the same places as the available observations from the TAO array (165°E , 180° , 170°W , 155°W , 140°W , 125°W , 110°W , and 95°W). We then use this subset of the model output to reconstruct the model currents, which gives us an indication of how accurately MM01 reconstructed the real currents from the limited observations. We can also diagnose which of their assumptions are, indeed, correct and which require some modification.

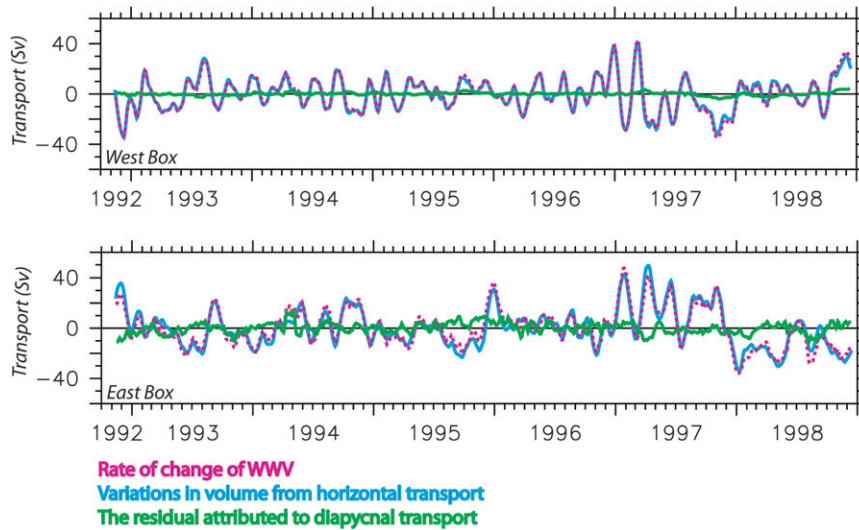


FIG. 5. Estimating diapycnal transports (Sv) using mass balance. The rate of change of the warm water volume ($dWWV/dt$, pink dashed line, calculated directly from the model output) and variations in the total horizontal volume transport above the pycnocline (cyan line), for the (top) west box and (bottom) east box, see Eq. (1). The residual between the two curves (green line) is an estimate of the diapycnal volume transport for each box. Negative values indicate anomalous downward transport. The mean values and the seasonal cycle have been removed from the time series. All variables are smoothed with a 10-point running mean.

MM01 approximate the meridional transport using the sum of the geostrophic and Ekman components:

$$\int_{165^{\circ}\text{E}}^{95^{\circ}\text{W}} \int_{\sigma_{\theta}=25}^{\text{surface}} v \, dz \, dx = \int_{165^{\circ}\text{E}}^{95^{\circ}\text{W}} \int_{\sigma_{\theta}=25}^{\text{surface}} \frac{p_x}{f\rho_0} \, dz \, dx - \int_{165^{\circ}\text{E}}^{95^{\circ}\text{W}} \int_{\sigma_{\theta}=25}^{\text{surface}} \frac{\tau_z^x}{f\rho_0} \, dz \, dx, \quad (2)$$

where p_x is the zonal pressure gradient, ρ_0 the average density, v the meridional velocity, f the Coriolis parameter, and τ_z^x is the zonal component of the vertical friction (integrating τ_z^x vertically gives the value of the wind stress applied at the surface). The first term is the geostrophic contribution and the second term is the Ekman transport. As an example, let us consider meridional transport through a transect along 5°N , extending from 165°E to 95°W , and from the instantaneous position of the 25.0 kg m^{-3} isopycnal up to the surface (as in our previous analysis).

First, we test whether geostrophy plus Ekman, excluding nonlinear advection and horizontal friction, is a good approximation to meridional transport in the model. For the Ekman component of flow above the pycnocline, we integrate the model's vertical friction between the surface and the isopycnal. In the central and western Pacific, the Ekman transport occurs above the thermocline and is captured fully by the integral of the vertical

friction. It appears that at 5°N geostrophy plus Ekman (green line in Fig. 7) are effective at reproducing the actual model meridional transport (black line). The rms error for this linear approximation is 5.0 Sv (see Table 1). However, while the two curves agree well, the error involved in these calculations is of a similar magnitude as the diapycnal transport that we are trying to find. Moreover, this estimate of meridional transport is more accurate than would be possible in the real ocean because here we use exact model pressure gradients and the knowledge of the depth of influence of the Ekman dynamics.

We now confine our analysis to the same data as would be used in an observational study and try to estimate model horizontal transports through the boundaries as defined in MM01. Two new assumptions are made: that all the Ekman transport occurs above the thermocline [the last term in Eq. (3)] and that estimates of dynamic height can be used to infer the zonal pressure gradient (rather than acquiring pressure directly from the model). The estimate of meridional transport along the transect is then

$$\int_{165^{\circ}\text{E}}^{95^{\circ}\text{W}} \int_{\sigma_{\theta}=25}^{\text{surface}} v \, dz \, dx = \int_{\sigma_{\theta}=25}^{\text{surface}} \frac{D[x=95^{\circ}\text{W}] - D[x=165^{\circ}\text{E}]}{f\rho_0} \, dz - \int_{165^{\circ}\text{E}}^{95^{\circ}\text{W}} \frac{\tau_z^x}{f\rho_0} \, dx, \quad (3)$$

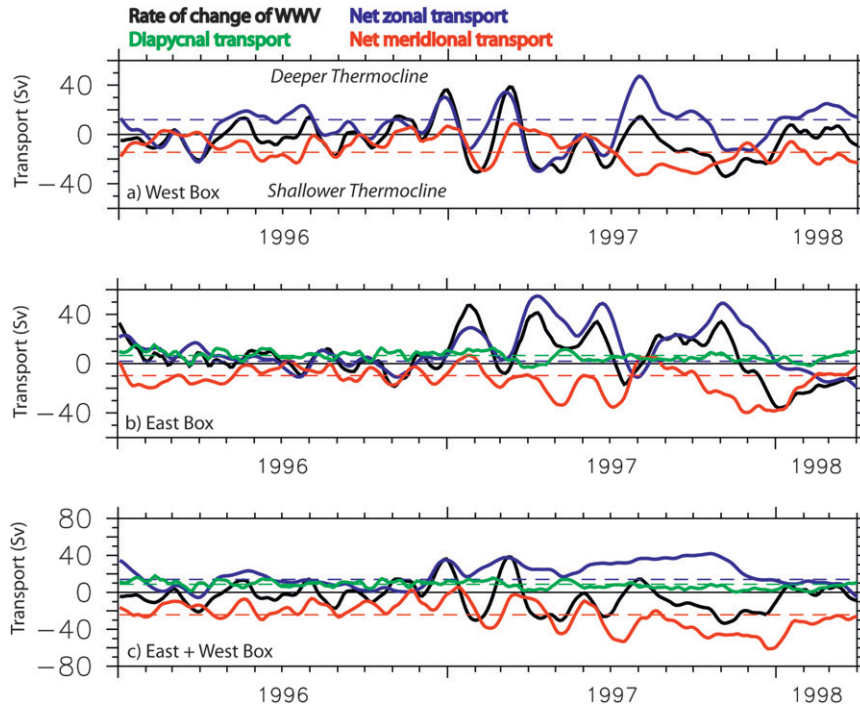


FIG. 6. Different contributions to the rate of change of WWV (black line) in the (a) west box, (b) east box, and (c) combined boxes before and during the 1997–98 El Niño: zonal transports (blue line), meridional transports (red line), and diapycnal transports (green line) (Sv). The mean strength of each transport is shown by the dashed line. The diapycnal volume transport for the west box is negligible and not shown. A 10-point running mean has been applied.

where D is dynamic height and τ^x is the wind stress. We calculate dynamic height from temperature and salinity profiles provided by the model. In MM01 salinity was not known, so the dynamic height was estimated using a technique that combined historical hydrography and heat content (Meinen and Watts 2000). The approximation in Eq. (3) (red line, Fig. 7) is not very different from the first assumption of geostrophy plus Ekman, as described by Eq. (2). The rms error remains similar at roughly 4.1 Sv. MM01 inferred that their method of estimating salinity would add another 2 Sv to this error.

In addition to these errors introduced in calculating dynamic heights, MM01 assumed a depth of no motion at 1000 dbar. Unable to quantify this error because there are very few observations at this depth, MM01 assumed it was small. Our estimates of meridional transport from the model pressure gradient and from a dynamic height estimate are so close that they support the depth of no motion assumption, as do the model's meridional velocities at 1000 m. This is not true, however, for zonal transports, which will be discussed later.

Part of the error in estimating the meridional transport comes from the Ekman approximation. In many places of the ocean, horizontal Ekman transport vanishes before the flow reaches the depth of the thermo-

cline. However, in the eastern equatorial Pacific, where the thermocline is very shallow (on the order of 30–50 m), the horizontal Ekman transport is below even the standard domain for the WWV (see Brown et al. 2007a). While small, this error is still significant when calculating residuals and small diapycnal velocities. This will also be apparent when we evaluate the extended Sverdrup relationship.

Now, to explore zonal transport estimates, we will look at the zonal flow across 165°E. This task is complicated by the fact that the Coriolis parameter goes to zero at the equator. Beyond 2° of latitude from the equator, the zonal velocity can be approximated by

$$\int u \, dz \, dy = \int \int_{\sigma_{\theta}=25}^{\text{surface}} \left(\frac{-p_y}{f\rho_0} + \frac{\tau_z^y}{f\rho_0} + \dots \right) dz \, dy \approx \int \int_{\sigma_{\theta}=25}^{\text{surface}} \frac{-D_y}{f\rho_0} dz \, dy + \int \frac{\tau^y}{f\rho_0} dy, \quad (4)$$

where we use the same notation as in Eq. (2) and introduce the zonal velocity u , the meridional pressure gradient p_y , and meridional component of wind stress τ^y . In this region, the Ekman transport is very small, $O(1 \text{ Sv})$. Away from the equator, the zonal velocity is

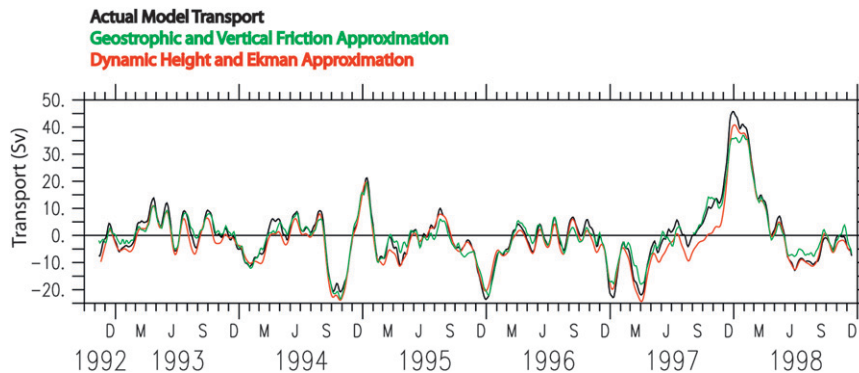


FIG. 7. Meridional transport (Sv) across 5°N between 165°E and 95°W calculated from different methods. The model's actual transport (black line) is compared to the estimates using the pressure gradient and vertical friction terms taken from the model output [green line; see Eq. (2)], and to the estimates using the dynamic height and Ekman transport approximations [red line; see Eq. (3)]. A 10-point running mean has been applied. The estimates are calculated using a spatial resolution comparable to the observations.

extremely well approximated by geostrophy, with a rms error of around 2 Sv (top and bottom panels of Fig. 8 and Table 1).

Within 2° of the equator we must use the y derivative of Eq. (4) (Picaut et al. 1989),

$$\int u \, dz \, dy = \int \int_{\sigma_{\theta=25}}^{\text{surface}} \left(\frac{-p_{yy}}{\beta\rho} + \frac{\tau_{zy}^y}{\beta\rho} + \dots \right) dz \, dy$$

$$\approx \int \int_{\sigma_{\theta=25}}^{\text{surface}} \frac{-D_{yy}}{f\rho_0} dz \, dy + \int \frac{\tau_y^y}{f\rho_0} dy, \quad (5)$$

where β is the meridional gradient of the Coriolis frequency at the equator. Using this approximation results in a rms error of 10.2 Sv (Fig. 8, middle panel).

Possible reasons to explain this large error include 1) this being a region of high nonlinearity (Kessler et al. 2003) or 2) flows may be complex, such as Yoshida jets (Cronin et al. 2000). It is also possible that our depth-of-no-motion assumption at 1000 m is the cause of the error. We tested this assumption by repeating the calculation with dynamic heights relative to 4000 rather than 1000 m (blue line, Fig. 8). Beyond 2° from the equator we found no discernible difference in the transport estimates. However, within the equatorial strip the revised calculations introduced changes of around 5 Sv, and the resulting rms error is reduced to 8.9 Sv. Furthermore, if we were interested in the total transport down to 1000 m, the reference level would become very important, with variability as large as 30 Sv, although the variations are minimized because we are considering flow only above the $25 \, \text{kg m}^{-3}$ isopycnal.

An alternative way to estimate meridional transport, without the need to calculate dynamic heights, is the extended Sverdrup balance (Kessler et al. 2003). As

shown in the appendix, in the equatorial region the depth-integrated meridional transport at any longitude obeys the equation

$$V = \frac{f}{\beta h} \frac{\partial h}{\partial t} + \frac{1}{\beta} \text{curl} \left(\frac{\tau^x}{\rho} \right) + \frac{1}{\beta} \text{curl}(\tau^{\text{NL},x})$$

$$- \frac{1}{\beta} \frac{\partial}{\partial t} (V_x - U_y), \quad (6)$$

where U , V are the depth-integrated meridional transports from the surface to h (the depth of the $25 \, \text{kg m}^{-3}$ isopycnal), τ^x is the zonal wind stress, and $\tau^{\text{NL},x} = \int [(uu)_x + (uv)_y + (uw)_z] dz$ is the zonal nonlinear advection term, as described in the appendix. The first term on the rhs of Eq. (6) can be thought of as the “vorticity stretching” term. It is related to changes in the thermocline depth at different distances away from the equator. The second term is the wind stress curl. The remaining two terms, which are highly complex in space and time, are referred to collectively as the “relative vorticity” terms. They describe much of the nonlinear features of the flow and the effect of ocean eddies.

Once again, we make a case study of the meridional transport across 5°N , between 165°E and 95°W above the pycnocline. The original (linear, steady) Sverdrup balance describes a meridional flow driven by the wind stress curl, that is, $V = \beta^{-1} \text{curl}(\tau^x)/\rho$, shown in Fig. 9a by the dashed black line. In earlier studies of the recharge–discharge oscillator, the change in WWV was attributed to this Sverdrup transport alone (e.g., Fig. 1 of Meinen and McPhaden 2000).

The volume transport given by the wind stress curl in the linear Sverdrup balance gives the full transport integrated from the surface to the bottom of the ocean.

TABLE 1. Rms error between actual model transports and a range of approximations. Zonal transport estimates are for flow across 165°E; meridional transport is across 5°N between 165°E and 95°W.

| Approximation to transport | Rms error compared to actual model transport (Sv) |
|---|---|
| Zonal transport approximations | |
| Geostrophic + Ekman (between 5° and 2° from equator) | 2.0 |
| Geostrophic + Ekman (within 2° of equator) relative to 1000 m | 10.2 |
| Geostrophic + Ekman (within 2° of equator) relative to 4000 m | 8.9 |
| Meridional transport approximations | |
| Full geostrophic + vertical friction [Eq. (2)] | 5.0 |
| Geostrophic (from dynamic height) + full Ekman [Eq. (3)] | 4.1 |
| Meridional transport – extended Sverdrup approximation | |
| Vertical friction curl only | 7.0 |
| Vertical friction + stretching | 5.3 |
| Vertical friction + stretching + relative vorticity | 4.4 |

Since we are considering flows above the pycnocline, we should compare the wind stress curl term to the curl of the vertical friction integrated from the surface to the 25 kg m⁻³ isopycnal (thick black line). The discrepancy between these two terms represents the influence of the wind stress curl below the pycnocline; it can be as large as 5 Sv at times.

In agreement with Clarke et al. (2007), both the wind stress curl and stretching term (red line, Fig. 9a) are important components of meridional transport, as are the nonlinear and relative vorticity terms (blue line). The actual model meridional transport (green line, Fig. 9b) is certainly not accounted for by the vertical friction curl alone (black line, Fig. 9b) nor is it much improved by including the stretching term (magenta line, Fig. 9b). However, when the extra relative vorticity terms are included (orange line, Fig. 9b), there is a much tighter match to the actual transport (Table 1).

The largest discrepancy occurs during the warm phases of the oscillation, especially during the onset of the strong 1997–98 El Niño when the wind stress curl and vorticity stretching term (magenta line, Fig. 9b) suggest that the northward transport is stronger and earlier than the actual values (green line, Fig. 9b). Therefore, if only the wind stress curl and vorticity stretching term were used to predict meridional transports, the estimated discharge would occur too early, but including the relative vorticity terms greatly improved the estimate of the meridional transport.

Even with these extra terms, the meridional transport estimate is not perfect and includes further assumptions and approximations. One reason for this remaining discrepancy is calculation errors that accumulate when integrating along the transect. For example, calculating a centered derivative on a grid is only an approximation to the actual derivative scheme used in the model.

Studying the balance at 5°S produces similar results, although the nonlinear terms south of the equator are

not as strong, as the tropical instability waves are typically weaker in the Southern Hemisphere.

4. Discussion and conclusions

Using the output of an ocean model, we have estimated the contribution of diapycnal transport to the variability of the warm water volume (WWV) in the equatorial Pacific as the residual of a mass balance above the 25.0 kg m⁻³ isopycnal. By using ocean model output we can accurately calculate the diapycnal contribution and avoid potential errors of observational studies. We find the contribution to be small or even negligible, compared to the variability of the horizontal transports. This finding is, however, clearly contingent on the fidelity of the ocean model. Ultimately, whether the real-ocean variations in diapycnal transport are indeed negligible on ENSO time scales remains to be confirmed with the next generation of ocean models or more comprehensive observations.

We estimate that interannual diapycnal flows across the pycnocline (25 kg m⁻³) were negligible in the west box (5°S–5°N, 156°E–140°W, see Figs. 3 and 5). In the east box (from 140°W to the American coast) the standard deviation of the diapycnal transport (with a 30-day running mean) is 4.2 Sv, while the rate of change of WWV had standard deviation of 15.4 Sv.

In contrast, similar, observational studies found that variability in the diathermal transports across the pycnocline was as large as that in the horizontal transports. MM01, for example, concluded that diathermal transports were important in both boxes, with values of up to 30 Sv in the 1998–99 La Niña (see their Fig. 13). Even with MM01's estimated error bound of 15 Sv, their results contradict our estimates. However, MM01's findings were reliant on approximations made in calculating the horizontal transports. Therefore, despite their best efforts, errors in such calculations were unavoidably folded into the approximation of the diathermal transport.

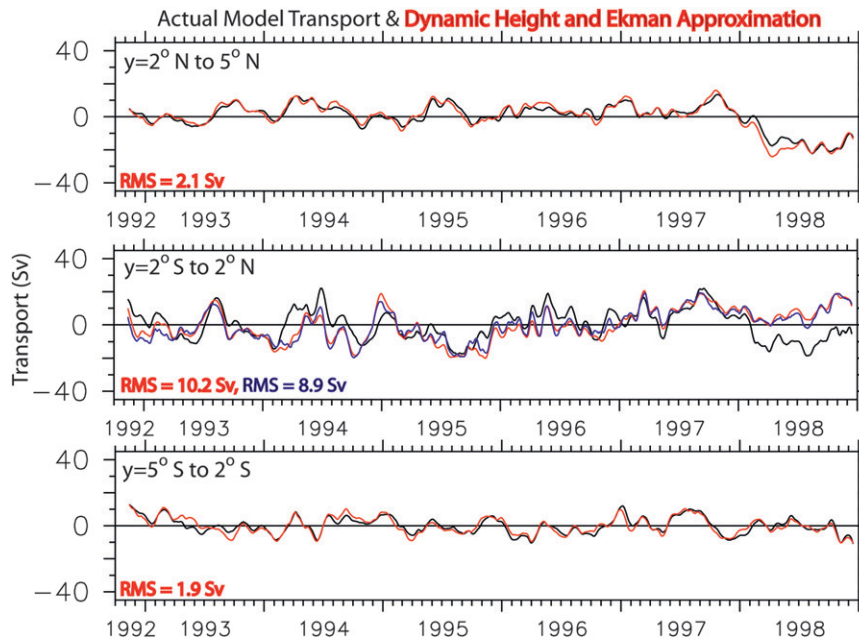


FIG. 8. Zonal transport (Sv) across 165°E calculated from different methods over three sections: (top) 2°N to 5°N , (middle) 2°S to 2°N , and (bottom) 5°S to 2°S . The model's actual zonal transports (black lines) are compared to estimates (red lines) based on the dynamic height (relative to 1000 m) and Ekman transport approximation. The middle panel also includes an estimate using dynamic heights calculated relative to 4000 m (blue line). The transports were estimated according to Eq. (4) except in the equatorial strip (2°S – 2°N) where Eq. (5) was used. A rms value is given in each between the actual model transport and the estimate. Plots smoothed with a 10-point running mean.

To explore possible sources of errors in the MM01 approach, we used our model output, sampled at the same locations as the TAO array, to emulate the MM01 study. We found that the meridional transports were fairly well reproduced when using only geostrophy and Ekman dynamics (as also found by Blanke and Raynaud 1997); however, the rms error across 5°N between 165°E and 95°W was 4.1 Sv (Fig. 7, Table 1). Errors in such estimates of the meridional transport could arise because, for example, the transport is not completely described by geostrophy and Ekman dynamics alone and may contain nonlinearities particularly owing to the presence of tropical instability waves. Those approximations also assume that the Ekman transport all occurs above the 25 kg m^{-3} isopycnal, which is not the case in the eastern part of the basin, where the thermocline is shallow (see Brown et al. 2007a). The assumption of the depth of no motion at 1000 m made no discernible difference to the transport estimates.

The largest source of error in our reconstruction of the WWV balance, emulating the MM01 study, proved to be from the geostrophic estimates of zonal transport (Fig. 8). The Ekman component of the zonal transport was of the order of only a few Sverdrups and was not

important. Beyond 2° from the equator, geostrophy alone was an effective description of the zonal transport: the rms error was 2 Sv. Within 2° of the equator, however, an equatorial geostrophy balance [Eq. (5)] led to large error estimates with a rms error of more than 10 Sv, giving a total error estimate at the western side of the tropical box as 10.6 Sv. MM01, who acknowledged this source of error, determined the rms errors in their calculation from TAO moorings (of the order of 11 Sv). We hypothesize that nonlinear and time-varying features were responsible for the inaccuracy. At this longitude, flow is highly complex because of westerly wind bursts and the constant readjusting of the ocean (Cronin et al. 2000).

In each transport estimate, the errors in our meridional transport and zonal transport estimates (5 Sv and 10.6 Sv) were much larger than the diapycnal transports that we were trying to estimate. (The variability of the diapycnal transport was, in some instances, larger than the error.) In the MM01 analysis, the error bars on their meridional, zonal, and diathermal transports were 9 Sv, 7 Sv, and 17 Sv, respectively. Thus, currently available observational arrays appear not to be adequate to assess the role of diapycnal transport in ENSO dynamics.

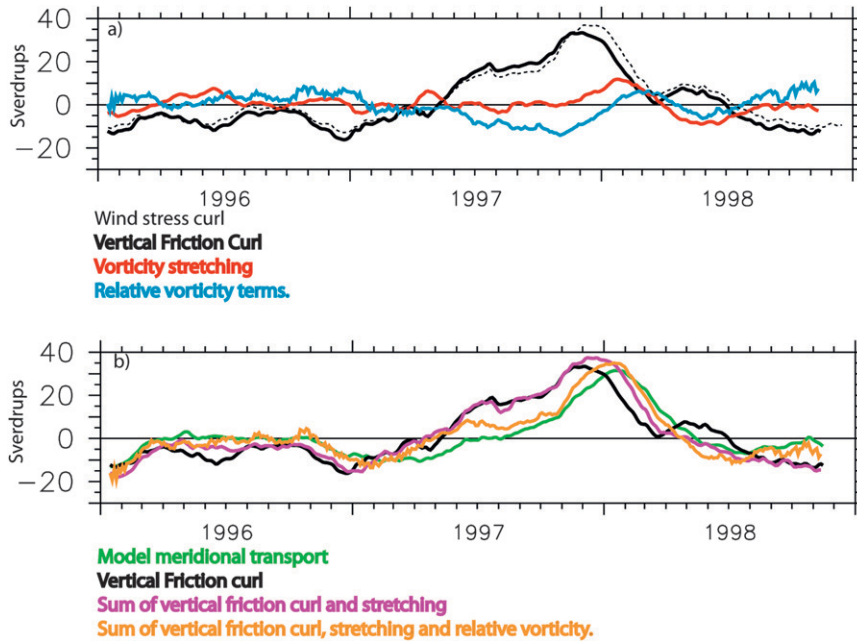


FIG. 9. (a) Physical terms contributing to the meridional transport across 5°N between 165°E and 95°W and from the surface to the instantaneous position of the 25 kg m^{-3} surface. The vertical friction curl (thick black line), the vortex stretching term (red line), and the relative vorticity terms [blue line; see Eq. (6)]. For comparison we show the linear Sverdrup transport given solely by the wind stress curl (black dashed line). (b) Estimates of the total meridional transport compared to the model's actual meridional volume transport (green line). The estimate from vertical friction curl alone (black line), the sum of vertical friction curl and stretching (magenta line), and the sum of the vertical friction term, stretching term, and relative vorticity terms (orange line). Each time series has been smoothed with a 31-point triangle filter. The model temporal resolution is 3 days and flow is shown in Sverdrups.

We have also explored the role of diapycnal transports for the long-term mean state of the ocean. Mean upwelling rates of 2.2 Sv were found for the west box and 6.6 Sv for the east box. MM01 found a mean diathermal upwelling across the 20°C isotherm for both boxes that was not statistically different from zero, though it had a standard error of 6 Sv. In that study the equatorial boxes extended from 8°S to 8°N , so their results are not exactly comparable to ours. In a later study (between 5°S and 5°N), Meinen et al. (2001) found evidence of upward diathermal transports at the thermocline. Above the thermocline this transport was much stronger, but beneath the thermocline the velocity was downward. Although Meinen et al. did not publish an integrated estimate for diathermal flow through the east box, their results for the mean transports appear to be of the same order of magnitude as ours. Bryden and Brady (1985) also found a relatively moderate diathermal upwelling across the 20°C isotherm, with downwelling at denser levels.

Iudicone et al. (2008) used a theoretical approach to estimate mean diapycnal transport. While using a larger box (10°S – 10°N , 170°W to the coast of South America),

they found a diapycnal transport of near 20 Sv across the 25 kg m^{-3} isopycnal and emphasized the role of short-wave radiation penetrating to this shallow isopycnal. Analyzing the role of surface heat fluxes lies beyond the scope of this paper, but it is an important way to assess models and compare the way they simulate ENSO events.

The volume balance that we calculated does not consider the role of precipitation and evaporation. MM01 found that including these effects would give a mean surface volume transport of around 0.05 Sv. They argue that, even if this estimate is an order of magnitude too small, the input through the ocean surface is still negligible compared to the total volume balance.

MM01's study differed from ours in that the thermocline was defined at the 20°C isotherm rather than the 25 kg m^{-3} isopycnal that we used. Both the 20°C isotherm in the observations and the 25 kg m^{-3} isopycnal in the model were effective demarcations for the pycnocline and, hence, give a good approximation for WWV. While we have taken great care to be consistent with the MM01 study, their different approach may account for some of our conflicting conclusions. For example,

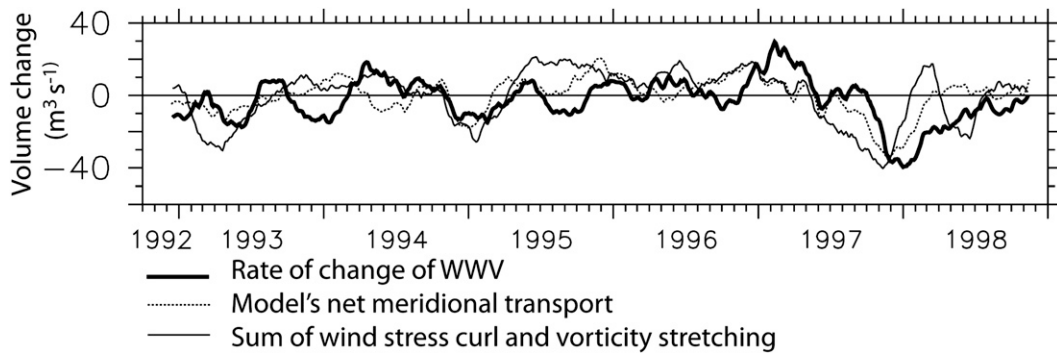


FIG. 10. The rate of change of warm water volume in the entire equatorial region; that is, east and west boxes combined (WWV, thick line). This rate cannot be accurately approximated by the meridional transport taken from the model (dashed line) or by the sum of the wind stress curl and vorticity stretching terms integrated over the northern and southern boundaries of the basin at 5°N and 5°S (thin line). Transports are shown in Sverdrups. Each time series has been smoothed with a 31-point triangle filter.

if a shallower isopycnal (*above* the 20°C isotherm) were taken, then stronger variations in vertical mass flux would be measured in the eastern part of the basin (not shown in this study). At shallower depths the anomalous vertical transport is clearly downward during El Niño and upward during La Niña (see Sun and Trenberth 1998; Wang and McPhaden 2000 for explanations of this process).

Although our results show small diapycnal transport across the pycnocline, they do not necessarily contradict the idea of the upwelling feedback relevant for ENSO dynamics (e.g., Jin and Neelin 1993; Fedorov and Philander 2001). Rather, they imply that on ENSO time scales the greatest changes in upwelling rates occur above the pycnocline [a conclusion supported by Bosc and Delcroix (2008), who found no connection between upwelling across the thermocline and ENSO phase]. These results do imply, however, that the upwelling feedback ought to be relatively weak since it would have to act on a relatively weak vertical temperature gradient.

To what extent might our results be model dependent, especially with regard to the mixing scheme used? There are a number of indicators of how well bulk mixing parameterizations work in the equatorial Pacific (e.g., Brown and Fedorov 2008): for example, how well the model captures the mean structure of the thermocline and the equatorial undercurrent (Fig. 1) or how well the model reproduces interannual variations in thermocline depth. To be as consistent as possible, we chose our WWV demarcation relative to the position of the model's pycnocline. We also demonstrated that the model WWV has a high correlation with observed WWV (Fig. 3). These aspects of the model were explored further in Brown (2005) and Brown et al. (2007a,b).

The original description of the recharge–discharge oscillator by Jin (1997) used coast-to-coast integrals so

that all of the recharge and discharge occurred due to meridional and not zonal transport. Although Clarke et al. (2007) later considered the tropical basin east of 156°E , which excludes western boundary currents and allows for zonal transport contributions, they still attributed the recharge and discharge of the equatorial Pacific solely to the meridional transports. Here, we have shown that meridional transports do not account for all of the variability in the WWV, and zonal transports driven by strong western boundary currents (MM01) should be taken into account (Fig. 6) (also see Alory and Delcroix 2002; Bosc and Delcroix 2008).

Both Jin (1997) and Clarke et al. (2007) use the Sverdrup balance to approximate meridional flows (the latter authors also add the vorticity stretching term to this balance). We have shown that approximating meridional transports only with Sverdrup transport and the vorticity stretching term introduces large errors (Fig. 9).

Why then do simple models that relate changes in WWV solely to Sverdrup transport, as does Clarke et al. (2007), seem to produce reasonable results, at least qualitatively? It appears that such an approach works well because both the wind stress curl and WWV have a strong ENSO signal so that one is merely a good proxy for the other (Fig. 10). Therefore, the Sverdrup balance approximation of the discharge and recharge remains adequate for conceptual models. However, for a more rigorous analysis of the mass balance, a careful treatment of all essential transport components should be used.

Coupled ocean–atmosphere GCMs vary greatly in how they reproduce the recharge and discharge of the equatorial Pacific (e.g., Mechoso et al. 2003; Guilyardi et al. 2009). The representation and relative importance of meridional and zonal transports in those models depend on a number of factors—from the simulated structure of the wind curl to the details of nonlinear terms in

the vicinity of the equator and from simulations of surface heating to the parameterizations of heat and momentum fluxes due to tropical instability waves. Ultimately, by changing the way the recharge and discharge occur, all of these factors can indirectly affect the properties of simulated ENSO as well as the relative role of diapycnal transports. Thus, assessing the relative roles of meridional, zonal, and diapycnal transports in coupled models, and their effect on ENSO, remains an important area of research.

Acknowledgments. We thank Drs. Andreas Schiller and Russell Fiedler from CSIRO, Australia, for providing the model output, Greg Johnson for the equatorial Pacific observational data, and Dr. Neville Smith, of BMRC Australia, for the gridded subsurface temperature data. Billy Kessler has been extremely helpful with critiques and suggestions for improvements. We also thank Dr. Trevor McDougall for advice and discussion on the physics of diapycnal transports and Chris Meinen for his useful suggestions. This research was supported in part by grants to AVF from NSF (OCE-0550439), DOE Office of Science (DE-FG02-06ER64238, DE-FG02-08ER64590), and the David and Lucile Packard Foundation.

APPENDIX

Equations for Meridional Transport

We begin with the three-dimensional, momentum and continuity equations for an incompressible ocean:

$$u_t + \mathbf{u} \cdot \nabla u - fv = \frac{-p_x}{\rho_0} + \frac{\tau_x^x}{\rho_0} + F^x \quad (\text{A1})$$

$$v_t + \mathbf{u} \cdot \nabla v + fu = \frac{-p_y}{\rho_0} + \frac{\tau_y^y}{\rho_0} + F^y \quad (\text{A2})$$

$$-(u_x + v_y) = w_z, \quad (\text{A3})$$

where u, v are the meridional and zonal velocities, $\mathbf{u} = (u, v, w)$, $\boldsymbol{\tau} = (\tau^x, \tau^y)$ as the shear stress (equal to the wind stress at the surface), $\mathbf{F} = (F^x, F^y)$ is the horizontal friction, $f = \beta y$ is the Coriolis parameter on the equatorial β plane, p is pressure, and ρ is density. The subscripts x, y, z , and t denote derivatives.

We take the horizontal curl of the momentum equations to obtain

$$-fw_z + \beta v + (v_x - u_y)_t = \frac{1}{\rho} \text{curl}(\boldsymbol{\tau}_z) + \text{curl}(\boldsymbol{\tau}_z^{\text{NL}}) + \text{curl}(\mathbf{F}_z), \quad (\text{A4})$$

where $\boldsymbol{\tau}^{\text{NL}}$ is the nonlinear advective terms. Following Kessler et al. (2003), it is defined as

$$\boldsymbol{\tau}^{\text{NL}} = \int \left((uu)_x + (uv)_y + (uw)_z, (vu)_x + (vv)_y + (vw)_z \right) dz,$$

where the integral is taken from the thermocline depth h to the surface. Note that Eq. (A4) is simply another form of the vorticity equation.

Integrating Eq. (A1) from the thermocline to the surface and rearranging yields

$$\beta V = \frac{1}{\rho} \text{curl}(\boldsymbol{\tau}) + \frac{f}{h} \frac{\partial h}{\partial t} + \text{curl}(\mathbf{F}) + \text{curl}(\boldsymbol{\tau}^{\text{NL}}) - (V_x - U_y)_t. \quad (\text{A5})$$

Here, we take

$$w = \frac{1}{h} \frac{Dh}{Dt} \approx \frac{1}{h} \frac{\partial h}{\partial t}$$

at the depth of the thermocline as a boundary condition for integrating. It is assumed that the horizontal derivatives of h are small (as outlined in Clarke et al. 2007). Simply, this is because the velocities are assumed to be nearly geostrophic (i.e., $fu = gh_y, fv = -gh_x$), so $f(uh_x + vh_y) = gh_y h_x - gh_x h_y = 0$. Previously, we argued that in the east Pacific the Ekman component is still significant at the thermocline. This assumption of geostrophy at the thermocline is one of the reasons for the discrepancies that remain in Fig. 9.

We have assumed that the vertical integral of $\boldsymbol{\tau}_z$ from the surface to the thermocline is equal to the total wind stress $\boldsymbol{\tau}$. This is a valid assumption in the central Pacific, but again not in the east. In the eastern Pacific, the thermocline depth is around 30–50 m, somewhat shallower than the penetration depth of the horizontal friction.

The balance between βV and the wind stress curl on the right side of Eq. (A5) is known as the Sverdrup balance. As it does not include nonlinearity and friction, the Sverdrup balance is inadequate for describing the flow (Kessler et al. 2003). It is also not applicable for nonsteady flows. The second term on the right side of Eq. (A5) is known as the ‘‘stretching term’’; it is significant between 5°N and 5°S (Clarke et al. 2007).

The curl of the horizontal friction (the third term) is small in the model that we are using (Brown et al. 2010); however, in other models it can be significant (Kessler et al. 2003), depending on the friction scheme used. The fourth term is the curl of the nonlinear advection term. For a steady state, Kessler et al. (2003) showed that along the equator, on annual mean, the curl of the nonlinear

term was as significant in the balance as the wind stress curl. In particular, the term represents the eastward advection of cyclonic relative vorticity found on the flanks of the Equatorial Undercurrent. At 5°N and S, the nonlinear curl diminishes, though Brown et al. (2010) show that tropical instability waves add a nonlinear signal at 5°N.

The final term is the rate of change of local relative vorticity $\zeta = v_x - u_y$. The last two terms of Eq. (A5) can be written together as a function of relative vorticity (before integrating with respect to depth),

$$\frac{D\zeta}{Dt} + \zeta(u_x + v_y) + \mathbf{k} \cdot \nabla_H w \times \frac{\partial \mathbf{u}}{\partial z}. \quad (\text{A6})$$

This comes about from taking the curl of $D\mathbf{u}/Dt$ in Eqs. (A1) and (A2). Clarke et al. (2007) argue that these terms are small on ENSO time scales and neglect them in their balance. However, according to our analysis, these terms in (A5) are important and cannot be neglected.

REFERENCES

- Alory, G., and T. Delcroix, 2002: Interannual sea level changes and associated mass transports in the tropical Pacific from TOPEX/Poseidon data and linear model results (1964–1999). *J. Geophys. Res.*, **107**, 3153, doi:10.1029/2001JC001067.
- Bentamy, A., N. Grimas, and Y. Quilfen, 1999: Validation of the gridded weekly and monthly wind fields calculated from ERS-1 scatterometer wind observations. *Global Atmos. Ocean Syst.*, **6**, 373–396.
- Blanke, B., and S. Raynaud, 1997: Kinematics of the Pacific Equatorial Undercurrent: An Eulerian and Lagrangian approach from GCM results. *J. Phys. Oceanogr.*, **27**, 1038–1053.
- Bosc, C., and T. Delcroix, 2008: Observed equatorial Rossby waves and ENSO-related warm water volume changes in the equatorial Pacific Ocean. *J. Geophys. Res.*, **113**, C06003, doi:10.1029/2007JC004613.
- Brown, J. N., 2005: The kinematics and dynamics of cross-hemispheric flow in the central and eastern equatorial Pacific. Ph.D. thesis, University of New South Wales, 216 pp.
- , and A. V. Fedorov, 2008: The mean energy balance in the tropical ocean. *J. Mar. Res.*, **66**, 1–23.
- , J. S. Godfrey, and R. Fiedler, 2007a: A zonal momentum balance on density layers for the central and eastern equatorial Pacific. *J. Phys. Oceanogr.*, **37**, 1939–1955.
- , —, and A. Schiller, 2007b: A discussion of cross-equatorial flow pathways in the central and eastern equatorial Pacific. *J. Phys. Oceanogr.*, **37**, 1321–1339.
- , —, and S. E. Wijffels, 2010: Nonlinear effects of tropical instability waves on the equatorial Pacific circulation. *J. Phys. Oceanogr.*, in press.
- Bryden, H. L., and E. C. Brady, 1985: Diagnostic model of the three-dimensional circulation in the upper equatorial Pacific Ocean. *J. Phys. Oceanogr.*, **15**, 1255–1273.
- Clarke, A. J., S. Van Gorder, and G. Colantuono, 2007: Wind stress curl and ENSO discharge/recharge in the equatorial Pacific. *J. Phys. Oceanogr.*, **37**, 1077–1091.
- Cronin, M. F., M. J. McPhaden, and R. H. Weisberg, 2000: Wind-forced reversing jets in the western equatorial Pacific. *J. Phys. Oceanogr.*, **30**, 657–676.
- Fedorov, A. V., and S. G. H. Philander, 2001: A stability analysis of the tropical ocean–atmosphere interactions: Bridging measurements of, and theory for El Niño. *J. Climate*, **14**, 3086–3101.
- Griffies, S. M., and R. W. Hallberg, 2000: Biharmonic friction with a Smagorinsky-like viscosity for use in a large-scale eddy-permitting ocean models. *Mon. Wea. Rev.*, **128**, 2935–2946.
- Guilyardi, E., A. Wittenberg, A. V. Fedorov, M. Collins, C. Wang, A. Capotondi, G. J. van Oldenborgh, and T. Stockdale, 2009: Understanding El Niño in ocean–atmosphere general circulation models: Progress and challenges. *Bull. Amer. Meteor. Soc.*, **90**, 325–340.
- Iudicone, D., G. Madec, and T. McDougall, 2008: Water-mass transformations in a neutral density framework and the key role of light penetration. *J. Phys. Oceanogr.*, **38**, 1357–1376.
- Jin, F. F., 1997: An equatorial ocean recharge paradigm for ENSO. Part I: Conceptual model. *J. Atmos. Sci.*, **54**, 811–829.
- , and J. D. Neelin, 1993: Modes of interannual tropical ocean–atmosphere interaction—A unified view. Part I: Numerical results. *J. Atmos. Sci.*, **50**, 3477–3503.
- , and S.-I. An, 1999: Thermocline and zonal advective feedbacks within the equatorial ocean recharge oscillator model for ENSO. *Geophys. Res. Lett.*, **26**, 2989–2992.
- Johnson, G. C., B. M. Sloyan, W. S. Kessler, and K. E. McTaggart, 2002: Direct measurements of upper ocean currents and water properties across the tropical Pacific during the 1990s. *Prog. Oceanogr.*, **52**, 31–61.
- Kessler, W. S., and B. A. Taft, 1987: Dynamic heights and zonal geostrophic transports in the central tropical Pacific during 1979–84. *J. Phys. Oceanogr.*, **17**, 97–122.
- , G. C. Johnson, and D. W. Moore, 2003: Sverdrup and nonlinear dynamics of the Pacific equatorial currents. *J. Phys. Oceanogr.*, **33**, 994–1008.
- Kleeman, R., and S. B. Power, 1995: A simple atmospheric model of surface heat flux for use in ocean modeling studies. *J. Phys. Oceanogr.*, **25**, 92–105.
- Mechoso, C., J. D. Neelin, and J.-Y. Yu, 2003: Testing simple models of ENSO. *J. Atmos. Sci.*, **60**, 305–318.
- Meinen, C. S., and M. J. McPhaden, 2000: Observations of warm water volume changes in the equatorial Pacific and their relationship to El Niño and La Niña. *J. Climate*, **13**, 3551–3559.
- , and D. R. Watts, 2000: Vertical structure and transport on a transect across the North Atlantic Current near 42°N: Time series and mean. *J. Geophys. Res.*, **105**, 21 869–21 891.
- , and M. J. McPhaden, 2001: Interannual variability in warm water volume transports in the equatorial Pacific during 1993–99. *J. Phys. Oceanogr.*, **31**, 1324–1345.
- , —, and G. C. Johnson, 2001: Vertical velocities and transports in the equatorial Pacific during 1993–99. *J. Phys. Oceanogr.*, **31**, 3230–3248.
- Meyers, G., H. Phillips, N. R. Smith, and J. Sprintall, 1991: Space and time scales for optimum interpolation of temperature—Tropical Pacific Ocean. *Prog. Oceanogr.*, **28**, 189–218.
- Niiler, P. P., and E. B. Kraus, 1977: One-dimensional models of the upper ocean. *Modelling and Prediction of the Upper Layers of the Ocean*, E. B. Kraus, Ed., Pergamon, 143–172.
- Pacanowski, R. C., and S. M. Griffies, 2000: MOM3 manual. NOAA/GFDL, 708 pp. [Available online at http://www.gfdl.noaa.gov/cms-filesystem-action/model_development/ocean/mom3_manual.pdf.]

- Picaut, J., S. P. Hayes, and M. J. McPhaden, 1989: Use of the geostrophic approximation to estimate time-varying zonal currents at the equator. *J. Geophys. Res.*, **94**, 3228–3236.
- Power, S., R. Kleeman, F. Tseitkin, and N. R. Smith, 1995: BMRC technical report on a global version of the GFDL modular ocean model for ENSO studies. Bureau of Meteorology, 18 pp.
- Schiller, A., 2004: Effects of explicit tidal forcing in an OGCM on the water-mass structure and circulation in the Indonesian throughflow region. *Ocean Modell.*, **6**, 31–49.
- , and J. S. Godfrey, 2003: Indian Ocean intraseasonal variability in an ocean general circulation model. *J. Climate*, **16**, 21–39.
- , —, P. C. McIntosh, G. Meyers, and S. E. Wijffels, 1998: Seasonal near-surface dynamics and thermodynamics of the Indian Ocean and Indonesian Throughflow in a global ocean general circulation model. *J. Phys. Oceanogr.*, **28**, 2288–2312.
- Smith, N. R., 1991: Objective quality controls and performance diagnostics of an oceanic subsurface thermal analysis scheme. *J. Geophys. Res.*, **96**, 3279–3287.
- , 1995a: The BMRC ocean thermal analysis system. *Aust. Meteor. Mag.*, **44**, 93–110.
- , 1995b: An improved system for tropical ocean sub-surface temperature analyses. *J. Atmos. Oceanic Technol.*, **12**, 850–870.
- , J. E. Blomley, and G. Meyers, 1991: A univariate statistical interpolation scheme for subsurface thermal analyses in the tropical oceans. *Prog. Oceanogr.*, **28**, 219–256.
- Sun, D.-Z., and K. E. Trenberth, 1998: Coordinated heat removal from the equatorial Pacific during the 1986–87 El Niño. *Geophys. Res. Lett.*, **25**, 2659–2662.
- Wang, W. M., and M. J. McPhaden, 2000: The surface-layer heat balance in the equatorial Pacific Ocean. Part II: Interannual variability. *J. Phys. Oceanogr.*, **30**, 2989–3008.